

# Laue diffraction of Mössbauer and x-ray photons in strongly absorbing crystals

A.Ya.Dzyublik, V.Yu.Spivak

Institute for Nuclear Research of the Ukrainian Academy of Sciences, avenue Nauki 47, 03680 Kiev, Ukraine

keywords: Mössbauer spectroscopy, Laue diffraction, dynamical scattering theory,  $\gamma$ -photon wave function, x-rays

## Abstract

The dynamical scattering theory is developed for the Laue diffraction of the Mössbauer rays and x-rays, whose angular distribution is comparable with the diffraction angular range. Both the Rayleigh and the resonant nuclear scattering are taken into account. We consider typical case when incident radiation first passes through an entrance slit and afterwards diffracts at the crystal planes within the Borrmann triangle. In calculations of the wave function for  $\gamma$ -photons, refracted or diffracted in such strongly absorbing crystal, we apply the saddle-point method. The distribution of their intensities over the basis of the Borrmann triangle is analyzed. In the spherical wave approximation of Kato, when aperture of the incident beam much exceeds the diffraction interval, the derived formulae well correlate with the familiar equations of the diffraction theory of X-rays.

## I. INTRODUCTION

The diffraction of x-rays, synchrotron radiation, Mössbauer rays and neutrons is widely used for analysis of crystal structure. In this way such unique phenomena were discovered as the pendellösung effect and the anomalous transmission of  $\gamma$ -photons and neutrons through a perfect crystal in the Laue (transmission) geometry. In the x-ray optics the latter effect is frequently referred to as the Borrmann effect [1-3]. The explanation of these phenomena has been given by the dynamical scattering theory [1-3]. In the two-wave case the incident plane x-ray wave generates inside the crystal two couples of waves, both of which are coherent superpositions of the transmitted and reflected waves. One such couple has nodes at the scattering atoms and is therefore anomalously weakly absorbed, whereas another, having antinodes, is strongly absorbed.

The dynamical scattering theory has been extended to the case of elastic diffraction of Mössbauer plane waves by Afanas'ev and Kagan [4]. They predicted that it can be realized complete suppression of  $\gamma$ -quanta by Mössbauer nuclei in perfect crystals, that was confirmed in numerous experiments.

Multiple scattering of x-ray photons by crystals is always described by the Maxwell equations [1-3]. In the same quasi-classical manner Afanas'ev and Kagan [4] treated the resonant scattering of Mössbauer radiation by a crystal. A quantum approach for the inelastic diffraction of  $\gamma$ -radiation in crystals, exposed to alternating external fields, has been presented in [5].

In typical Laue-diffraction experiments the incident  $\gamma$ -quanta are first collimated by a slit, lying on the crystal surface and being parallel to the reflecting planes (see Fig.1). And after that the radiation flows within the angular region, which forms a so-called Borrmann triangle (fan). The intensity distribution of the transmitted and reflected beams over the basis of the Borrmann triangle is analyzed with the aid of one more slit, which is also parallel to the reflecting crystal planes.

Standard plane-wave dynamical theory is not able to describe this situation. Therefore Kato [6] considered the Laue diffraction of x-ray spherical waves, treating them like a superposition of the classical plane waves, which spread over the angle  $\theta$  about the Bragg angle  $\theta_B$ . Every such plane component independently of each other are scattered by atoms of the crystal, forming the refracted and diffracted wave packets, represented by the integrals over the angle  $\theta$ . In such a spherical-wave approximation it was silently believed that the dispersion  $\sigma$  of the incident rays over  $\theta$  much exceeds the characteristic angular interval  $|\Delta\theta|$ , where the diffraction proceeds. Kato found exact solution of the integral over  $\theta$  in terms of the Bessel function. Besides, these integrals can be estimated over  $\theta$  with the aid of the stationary-phase approximation if the crystal thickness  $D$  to be much larger than the pendellösung length  $\Lambda_L$  [3]. This method, however, can be used only if the large parameter of the task  $D/\Lambda_L$  is a real number. In other words, it can be applied only to weakly absorbing crystals.

At the same time, for the Mössbauer diffraction, when the resonant scattering amplitude of  $\gamma$ -quanta is already a complex number, the stationary-phase method is not applicable. In this case such integrals should be estimated in

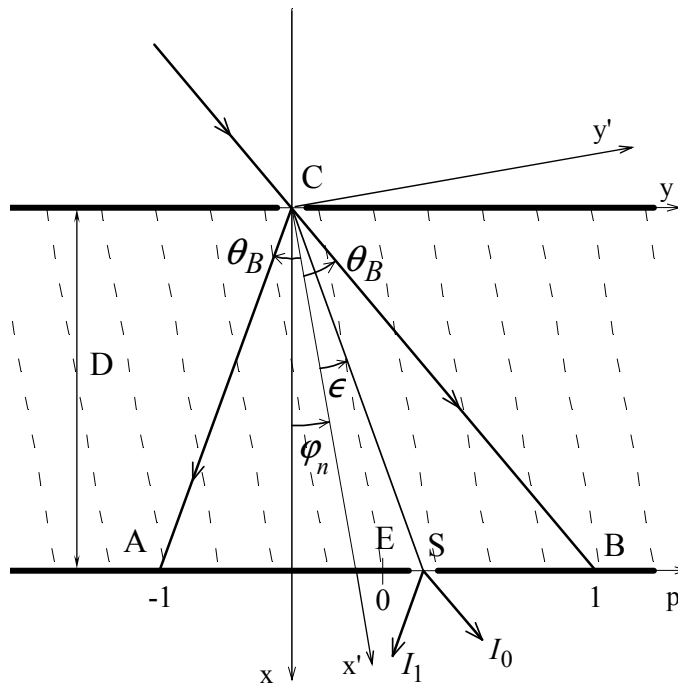


FIG. 1: Scheme of the Laue diffraction of the collimated  $\gamma$ -rays, whose flow is concentrated mainly inside the Borrmann triangle ABC. The points A and B are marked by the reduced coordinates  $p = -1$  and  $p = 1$ , respectively; the middle point E of the line segment AB by  $p = 0$ . The collimating and scanning slits are labeled by C and S, respectively. The reflecting planes are drawn by the dashed lines.

more general saddle-point approach. Previously we did this in the spherical-wave approximation, confining ourselves with the symmetric Laue diffraction of both Mössbauer radiation [7] and neutrons [8].

Now we analyze much more general case of the Mössbauer diffraction in arbitrary Laue geometry, when the dispersion  $\sigma$  may be of the order of the diffraction range  $|\Delta\theta|$ . In our calculations we describe photons by the vector wave function  $\Psi(\mathbf{r}, t)$  suggested by Bialynicki-Birula [10]. It is represented by the wave packet, composed by the plane waves  $\chi_{\kappa\lambda}(\mathbf{r})e^{-i\omega t}$ , where

$$\chi_{\kappa\lambda}(\mathbf{r}) = \mathbf{e}_\lambda(\boldsymbol{\kappa})\sqrt{\hbar\omega}e^{i\boldsymbol{\kappa}\mathbf{r}} \quad (1)$$

with the wave vector  $\boldsymbol{\kappa}$ , helicity  $\lambda = \pm 1$  and frequency  $\omega = c\kappa$ . The modulus squared of  $\Psi(\mathbf{r}, t)$  is now interpreted as a probability density of detecting the photon's mean energy at the given position  $\mathbf{r}$  in the moment  $t$ . Application of such a wave function allows us to employ quantum scattering theory [11, 12] for analysis of the diffraction of  $\gamma$ -quanta.

## II. SCATTERING AMPLITUDES

We introduce the right-hand coordinate frame  $x, y, z$  with the origin on the entrance surface in the middle of the collimating slit. The axis  $x$  is directed inside the crystal perpendicularly to its surface and the axis  $z$  along the slit (see Fig.1). One introduces also the frame  $x', y', z'$  with the axis  $x'$  parallel to the reflecting crystal planes and axis  $z'$  coinciding with  $z$ . It is obtained from  $x, y, z$  by rotation through the angle  $\varphi_n$  around the axis  $z$ . Here  $\varphi_n < 0$  for clockwise rotation and  $\varphi_n > 0$  otherwise. The angle between the photon wave vector  $\boldsymbol{\kappa}$  and the axis  $x$  is  $\varphi$ , the incidence angle on the reflecting planes is  $\theta$ , the Bragg angle  $\theta_B$ .

In addition, we introduce the angles  $\varphi_0$  and  $\varphi_1$  between the axis  $x$  and the sides of the Borrmann triangle,  $\varphi_0 = \theta_B + \varphi_n > 0$  and  $\varphi_1 = -\theta_B + \varphi_n < 0$ .

Let the divergent beam of  $\gamma$ -quanta move in the plane  $x, y$  perpendicularly to the slit and be spread over the angle  $\theta$ . Then the components of  $\boldsymbol{\kappa}(\theta)$ , written in cylindrical coordinates, are

$$\boldsymbol{\kappa}(\theta) = \{\kappa \cos \varphi, \kappa \sin \varphi, 0\}, \quad (2)$$

where  $\varphi = \varphi_n + \theta$ .

The wave function of the incident photon may be written as

$$\Psi_s(\mathbf{r}, t)_{\text{in}} = \int_0^\infty G_e(\omega) \Psi_{\omega,s}(\mathbf{r})_{\text{in}} e^{-i\omega t} d\omega, \quad (3)$$

where  $G_e(\omega)$  specifies the frequency distribution of the incident photons, the function

$$\Psi_{\omega,s}(\mathbf{r})_{\text{in}} = \int_{-\pi}^\pi G_a(\theta) \chi_{\kappa(\theta)s}(\mathbf{r}) d\theta \quad (4)$$

describes photons with fixed frequency  $\omega$  and polarization  $\mathbf{e}_s$ . The polarization vectors  $\mathbf{e}_s(\boldsymbol{\kappa})$  are perpendicular to the wave vector  $\boldsymbol{\kappa} = \kappa(\theta)$  and therefore also depend on the angle  $\theta$ . However, one can neglect this dependence since the dispersion  $\sigma \ll 1$ .

We approximate the angular distribution by the Gaussian function, concentrated at the angle  $\theta_0$  close to the Bragg angle  $\theta_B$ :

$$G_a(\theta) = \frac{1}{(\sqrt{2\pi}\sigma)^{1/2}} \exp\left\{-\frac{(\theta_0 - \theta)^2}{4\sigma^2}\right\}, \quad (5)$$

where

$$\sigma^2 = \langle (\theta_0 - \theta)^2 \rangle \quad (6)$$

denotes the mean-square angular distribution of the beam. Usually  $\sigma \ll 1$ , that enables us to spread the integration limits over  $\theta$  from  $-\infty$  to  $\infty$ . In the spherical-wave approximation of Kato this distribution is replaced by unity.

In general case polarizations of  $\gamma$ -quanta are mixed during the resonant scattering by nuclei. Below we only consider scattering by unpolarized Mössbauer nuclei with unsplit sublevels, labeled by the magnetic quantum number. In this case the mixing is avoided if  $\gamma$ -quanta have either  $\pi$ -polarization  $\mathbf{e}_{s=1}$ , lying in the scattering plane or  $\sigma$ -polarization  $\mathbf{e}_{s=2}$ , being perpendicular to this plane [13].

The frequency distribution for the phononless emission line is determined by the function

$$G_e(\omega) = \left(\frac{\Gamma_e}{2\pi\hbar}\right)^{1/2} \frac{e^{i\omega t_0}}{\omega - \omega_e + i\Gamma_e/2\hbar}, \quad (7)$$

where  $\Gamma_e$  and  $\hbar\omega_e$  are respectively the width and energy of the excited level of the emitting nucleus. Time dependence of the incident  $\gamma$ -quantum at the entrance surface ( $x = 0$ ) is described by the exponential:

$$|\Psi_{\text{in}}^{(s)}(0, t)|^2 \sim \exp[-\Gamma_e(t - t_0)/\hbar]\theta(t - t_0), \quad (8)$$

where

$$\theta(x) = \begin{cases} 1, & x > 0, \\ 0, & x < 0. \end{cases} \quad (9)$$

is the Heaviside step function. According to (8)  $t_0$  means the moment of the photon's arrival to the crystal.

The coherent scattering amplitude of  $\gamma$ -quanta by the  $j$ th nucleus with unsplit sublevels is given by [13]

$$f_{\text{coh}}(\boldsymbol{\kappa}, \mathbf{e}_s; \boldsymbol{\kappa}', \mathbf{e}'_s)_j^N = -c_0 \left(\frac{2I_e + 1}{2I_g + 1}\right) \frac{1}{4\kappa} \frac{\Gamma_\gamma e^{-W_j(\boldsymbol{\kappa}) - W_j(\boldsymbol{\kappa}')}}{\hbar(\omega - \omega'_0) + i\Gamma/2} P_s^N, \quad (10)$$

where  $c_0$  is the relative concentration of the Mössbauer isotope,  $I_e$  and  $I_g$  are the nuclear spins in the excited and ground states,  $e^{-W_j(\mathbf{k})}$  is the Lamb-Mössbauer factor,  $P_s^N$  is the nuclear polarization factor,  $\Gamma$  and  $\Gamma_\gamma$  are respectively the total and radiative widths of the resonant nuclear level with the energy  $\hbar\omega'_0$ . In the case of M1 transitions  $P_s^N = 1$  for the  $\pi$ -polarization, and  $P_s^N = \mathbf{e} \cdot \mathbf{e}'$  for the  $\sigma$ -polarization [13].

The coherent Rayleigh scattering amplitude by the  $j$ th atom is determined by the expression

$$f_{\text{coh}}(\boldsymbol{\kappa}, \mathbf{e}_s; \boldsymbol{\kappa}', \mathbf{e}'_s)_j^R = e^{-W_j(\mathbf{Q})} r_0 F_e^{(j)}(\mathbf{Q})(\mathbf{e}_s \cdot \mathbf{e}'_s^*) + (\kappa/4\pi)\sigma_e^{(j)}, \quad (11)$$

where the form-factor of the  $j$ th atom

$$F_e^{(j)}(\mathbf{Q}) = \int \varrho_e^{(j)}(\mathbf{r}) e^{i\mathbf{Q}\mathbf{r}} d\mathbf{r}, \quad (12)$$

$\mathbf{Q} = \boldsymbol{\kappa} - \boldsymbol{\kappa}'$  is the scattering vector,  $\rho_e^{(j)}(\mathbf{r})$  is the density of atomic electrons,  $r_0 = e^2/mc^2$  denotes the classical radius of the electron,  $\sigma_e^{(j)}$  is the absorption cross section of  $\gamma$ -quanta by electrons of the  $j$ th atom.

The coherent scattering amplitude of  $\gamma$ -quanta by elementary cell of the crystal

$$F_{\text{coh}}(\boldsymbol{\kappa}, \mathbf{e}; \boldsymbol{\kappa}', \mathbf{e}') = F_{\text{coh}}(\boldsymbol{\kappa}, \mathbf{e}; \boldsymbol{\kappa}', \mathbf{e}')^N + F_{\text{coh}}(\boldsymbol{\kappa}, \mathbf{e}; \boldsymbol{\kappa}', \mathbf{e}')^R, \quad (13)$$

where

$$F_{\text{coh}}(\boldsymbol{\kappa}, \mathbf{e}; \boldsymbol{\kappa}', \mathbf{e}')^{N(R)} = \sum_j e^{i\mathbf{Q}\boldsymbol{\rho}_j} f_{\text{coh}}(\boldsymbol{\kappa}, \mathbf{e}; \boldsymbol{\kappa}', \mathbf{e}')_j^{N(R)} \quad (14)$$

are the nuclear and Rayleigh coherent scattering amplitudes, depending on the radius vector  $\boldsymbol{\rho}_j$  for the equilibrium position of the  $j$ th atom in the elementary cell.

### III. DYNAMICAL SCATTERING THEORY

Every plane component  $\chi_{\boldsymbol{\kappa}(\theta),s}(\mathbf{r})$  of the incident wave packet (4) is scattered independently, generating the wave  $\psi_{\boldsymbol{\kappa}(\theta),s}(\mathbf{r})$  [11]. As a consequence, the complete wave function of the photon will be

$$\Psi_s(\mathbf{r}, t) = \int_{-\infty}^{\infty} d\omega G_e(\omega) \int_{-\infty}^{\infty} d\theta G_a(\theta) \psi_{\boldsymbol{\kappa}_s}(\mathbf{r}) e^{-i\omega t} \quad (15)$$

with the same distributions  $G_e(\omega)$  and  $G_a(\theta)$  as the incident wave packet (3), (4).

In the two-wave diffraction the wave  $\psi_{\boldsymbol{\kappa}(\theta)}(\mathbf{r})$  inside the crystal as  $0 < x < D$ , where  $D$  is the crystal thickness, consists of the refracted wave with the wave vector  $\mathbf{k}(\theta)$  and the diffracted one with the wave vector  $\mathbf{k}_1(\theta) = \mathbf{k}(\theta) + \mathbf{h}$ , where  $\mathbf{h}$  denotes a reciprocal lattice vector. The components of the vectors  $\mathbf{k}(\theta)$  and  $\boldsymbol{\kappa}(\theta)$  along the entrance surface  $x = 0$  coincide and therefore

$$\mathbf{k}_\nu(\theta) = \boldsymbol{\kappa}_\nu(\theta) + \delta(\theta)\mathbf{n}, \quad \mathbf{k}_1(\theta) = \boldsymbol{\kappa}_0(\theta) + \mathbf{h}, \quad (16)$$

where  $\mathbf{n}$  is the unit vector along the axis  $x$ .

As a consequence, the wave function  $\Psi_{\omega s}(\mathbf{r})$  inside the crystal transforms to

$$\Psi_{\omega s}(\mathbf{r}) = \sum_{\nu=0,1} \Psi_{\omega s}^{(\nu)}(\mathbf{r}), \quad (17)$$

where

$$\Psi_{\omega s}^{(\nu)}(\mathbf{r}) = \int_{-\infty}^{\infty} d\theta G_a(\theta) \psi_{\boldsymbol{\kappa}_\nu(\theta),s}(\mathbf{r}) \quad (18)$$

with  $\psi_{\boldsymbol{\kappa}_\nu(\theta),s}(\mathbf{r})$  given by

$$\psi_{\boldsymbol{\kappa}_\nu(\theta),s}(\mathbf{r}) = \mathbf{e}_{\nu s} \sqrt{\hbar\omega} \sum_{\iota=1,2} C_{\nu s}^{(\iota)}(\theta) e^{i\boldsymbol{\kappa}_\nu(\theta)\mathbf{r} + i\delta_{\iota s}(\theta)x}. \quad (19)$$

For the two-wave case the amplitudes  $C$  and the wave vectors  $\mathbf{k}$  are determined by equations [4]

$$\begin{aligned} (k^2(\theta)/\kappa^2(\theta) - 1)C_0 &= g_{00}C_0 + g_{01}^{(s)}C_1, \\ (k_1^2(\theta)/\kappa^2(\theta) - 1)C_1 &= g_{10}^{(s)}C_0 + g_{11}C_1. \end{aligned} \quad (20)$$

The scattering matrix  $g_{\mu\nu}^{(s)}$  is defined by the expression

$$g_{\mu\nu}^{(s)} = \frac{4\pi}{\kappa^2 v_0} F(\boldsymbol{\kappa}_\nu, \mathbf{e}_{\nu s}; \boldsymbol{\kappa}_\mu, \mathbf{e}_{\mu s}), \quad \mu, \nu = 0, 1, \quad (21)$$

where  $v_0$  stands for the volume of the elementary cell.

The system of two equations (20) has the following solution [4]:

$$\delta_{1,2}^{(s)} = \kappa \varepsilon_{0s}^{(1,2)} / \gamma_0, \quad (22)$$

where

$$\varepsilon_{0s}^{(1,2)} = \frac{1}{4} [g_{00} + \beta g_{11} - \beta \alpha] \pm \frac{1}{4} \left\{ [g_{00} + \beta g_{11} - \beta \alpha]^2 + 4\beta \left[ g_{00}\alpha - (g_{00}g_{11} - g_{01}^{(s)}g_{10}^{(s)}) \right] \right\}^{1/2}, \quad (23)$$

with

$$\beta = \gamma_0/\gamma_1, \quad \alpha = \frac{2\kappa(\theta)\mathbf{h} + \mathbf{h}^2}{\kappa^2}, \quad \gamma_\nu = \cos \varphi_\nu. \quad (24)$$

The angle  $\alpha$  defines deviation from the exact Bragg condition  $\kappa_1 = \kappa$ . For photons with fixed frequency [1]

$$\alpha = 2 \sin 2\theta_B \Delta\theta, \quad (25)$$

where

$$\Delta\theta = \theta_B - \theta. \quad (26)$$

It is most convenient to express  $\varepsilon_0^{(1,2)}$  in terms of new deviation parameter

$$\eta = \frac{1}{2} \left( \frac{\beta}{g_{01}^{(s)}g_{10}^{(s)}} \right)^{1/2} (\alpha - \alpha_0), \quad (27)$$

where the angular shift

$$\alpha_0 = g_{11} - g_{00}/\beta. \quad (28)$$

Notice that  $\alpha_0$  diminishes in the case of symmetric diffraction,  $\beta = 1$ , if  $g_{11} = g_{00}$ .

Making use of the above definitions we transform the parameter  $\delta_l(\eta)$ , defined by Eqs.(22), (23), to

$$\delta_l^{(s)}(\eta) = \frac{\kappa g_{00}}{2\gamma_0} - \frac{\pi}{\Lambda_L} \left[ \eta + (-1)^{l+1} \sqrt{1 + \eta^2} \right], \quad (29)$$

where

$$\Lambda_L = \frac{2\pi\gamma_0}{\kappa \sqrt{g_{01}^{(s)}g_{10}^{(s)}}\beta} \quad (30)$$

means the Pendellösung distance in the case of weakly absorbing crystals (see, e.g., [3]).

For the Laue diffraction ( $\beta > 0$ ) the amplitudes of the waves satisfy the following boundary conditions at  $x = 0$ :

$$\sum_{\iota=1,2} C_{0s}^{(\iota)}(\theta) = 1, \quad \sum_{\iota=1,2} C_{1s}^{(\iota)}(\theta) = 0. \quad (31)$$

Being expressed in terms of  $\eta$ , these amplitudes take the form

$$C_{0s}^{(\iota)}(\eta) = \frac{1}{2} \left[ 1 + (-1)^\iota \frac{\eta}{\sqrt{1+\eta^2}} \right], \quad C_{1s}^{(\iota)}(\eta) = \frac{(-1)^\iota}{2} \left( \frac{g_{10}^{(s)}}{g_{01}^{(s)}} \right)^{\frac{1}{2}} \sqrt{\frac{\beta}{1+\eta^2}}. \quad (32)$$

Combining Eqs. (25) and (27), one finds the relation between our departure parameters:

$$\Delta\vartheta\eta = \theta'_B - \theta, \quad (33)$$

where

$$\Delta\vartheta = \frac{1}{\sin 2\theta_B} \sqrt{\frac{g_{01}^{(s)}g_{10}^{(s)}}{\beta}}, \quad \theta'_B = \theta_B + \Delta\theta_B, \quad \Delta\theta_B = -\frac{\alpha_0}{2 \sin 2\theta_B}. \quad (34)$$

From (33) we see that  $|\Delta\vartheta|$  implies a characteristic diffraction interval, where  $|\eta| \leq 1$ , while  $\theta'_B$  stands for the corrected Bragg angle corresponding to  $\eta = 0$ . The above formulas can be also rewritten as

$$\Delta\theta = \frac{\alpha_0}{2 \sin 2\theta_B} + \Delta\vartheta\eta. \quad (35)$$

Using the parameters introduced above one can transform the expression (18) for the wave function to

$$\Psi_{\omega_S}^{(\nu)}(\mathbf{r}) = -\sqrt{\Delta\vartheta} \int_{-\infty}^{\infty} d\eta \mathcal{G}_a(\eta) \psi_{\kappa_\nu(\theta),s}(\mathbf{r}). \quad (36)$$

Now the angular distribution versus  $\eta$  is given by

$$\mathcal{G}_a(\eta) = \frac{1}{(2\pi\bar{\eta}^2)^{1/4}} \exp\left\{-\frac{(\eta - \Delta\eta)^2}{4\bar{\eta}^2}\right\}, \quad (37)$$

where the parameter

$$\Delta\eta = \frac{\theta'_B - \theta_0}{\Delta\vartheta} \quad (38)$$

characterizes a mismatch of the beam orientation and the Bragg resonance, and

$$\bar{\eta}^2 = (\sigma/\Delta\vartheta)^2 \quad (39)$$

specifies a squared width of the distribution.

The intensity distribution over the basis of the Borrmann triangle is usually analyzed with the aid of the scanning slit, located on the rear surface and directed along the axis  $z$ . Let this slit cross the axis  $y$  in the point  $y_S$ , while the midpoint E on the basis AB of the Borrmann triangle have the coordinate  $y_0$ . It is convenient to introduce the reduced coordinate  $p$  of the scanning slit determined by

$$p = \frac{\Delta y_S}{L}, \quad (40)$$

where  $2L$  is the length of the line segment AB and  $\Delta y_S = y_S - y_0$  stands for the shift of the scanning slit with respect to the center of the Borrmann triangle basis. The analogous definition of this reduced coordinate was given by Authier [3]. The definition (40) is equivalent to

$$p = 2 \frac{\Delta y_S/D}{\tan \varphi_0 - \tan \varphi_1}, \quad (41)$$

which in the case of symmetric diffraction, as  $\beta = 1$ , reduces to the definition of  $p$ , given in Refs. [2, 6]:

$$p = \frac{\tan \epsilon}{\tan \theta_B}, \quad (42)$$

where  $\epsilon$  is the angle between the reflecting planes and the direct line CS, connecting the entrance and exit slits (see Fig. 1).

Let us expand now the exponent of the  $e^{i\kappa(\theta)\mathbf{r}}$  in  $\Delta\theta$ :

$$e^{i\kappa_\nu(\theta)\mathbf{r}} \approx \exp\left\{i\kappa \sin \varphi_0 D \left[1 - \frac{y_S/D}{\tan \varphi_0}\right] \Delta\theta\right\} e^{i\kappa_\nu \mathbf{r}}. \quad (43)$$

Here

$$\frac{y_S/D}{\tan \varphi_0} = \frac{1}{\tan \varphi_0} \left[ \frac{\tan \varphi_0 + \tan \varphi_1}{2} + \frac{\tan \varphi_0 - \tan \varphi_1}{2} p \right]. \quad (44)$$

From the equalities

$$\varphi_0 + \varphi_1 = 2\varphi_n, \quad \varphi_0 - \varphi_1 = 2\theta_B \quad (45)$$

it follows that

$$\tan \varphi_0 + \tan \varphi_1 = \frac{\sin 2\varphi_n}{\gamma_0 \gamma_1} \quad (46)$$

and

$$\tan \varphi_0 - \tan \varphi_1 = \frac{\sin 2\theta_B}{\gamma_0 \gamma_1}. \quad (47)$$

This allows us to transform (44) as

$$\frac{y_S/D}{\tan \varphi_0} = \frac{1}{2 \tan \varphi_0} \left[ \frac{\sin 2\varphi_n + p \sin 2\theta_B}{\gamma_0 \gamma_1} \right]. \quad (48)$$

By making use of the relation

$$\sin 2\varphi_n + \sin 2\theta_B = 2 \sin \varphi_0 \gamma_1 \quad (49)$$

one gets

$$\frac{y_S/D}{\tan \varphi_0} = 1 + \frac{\sin \theta_B \cos \theta_B}{\sin \varphi_0 \gamma_1} (p - 1). \quad (50)$$

With this formula and Eq. (35) we transform Eq. (43) to

$$\exp\{i\boldsymbol{\kappa}_\nu(\theta)\mathbf{r}\} = \exp\left\{i\frac{\kappa D}{4\gamma_1}(1-p)\alpha_0\right\} \exp\left\{i\frac{\pi D}{\Lambda_L}(1-p)\eta\right\} e^{i\boldsymbol{\kappa}_\nu\mathbf{r}}.$$

Taking also into account Eq. (29), we are led to the following expression for the plane waves at the exit slit, i.e., at  $\mathbf{r} \approx \{D, y_S, 0\}$ :

$$\exp\{i\boldsymbol{\kappa}_\nu(\theta)\mathbf{r} + i\delta_l(\theta)D\} = \Phi(p; \omega) \exp\left\{-i\frac{\pi D}{\Lambda_L} \left[ p\eta + (-1)^{\iota+1} \sqrt{1 + \eta^2} \right]\right\} e^{i\boldsymbol{\kappa}_\nu\mathbf{r}},$$

where we used the abbreviation

$$\Phi(p; \omega) = \exp\left\{i\frac{\kappa D}{4} \left[ \frac{g_{00}}{\gamma_0} + \frac{g_{11}}{\gamma_1} + p \left( \frac{g_{00}}{\gamma_0} - \frac{g_{11}}{\gamma_1} \right) \right]\right\}. \quad (51)$$

Inserting (51) into (36) we represent the photon wave functions as

$$\boldsymbol{\Psi}_{\omega,s}^{(\nu)}(\mathbf{r}) = -\sqrt{\hbar\omega}\mathbf{e}_s\Phi(p; \omega)\sqrt{\Delta\vartheta} \sum_{\iota=1,2} \mathcal{I}_{\nu s}^{(\iota)} e^{i\boldsymbol{\kappa}_\nu\mathbf{r}}, \quad (52)$$

where  $\mathcal{I}_{\nu s}^{(\iota)}$  denotes the integral

$$\mathcal{I}_{\nu s}^{(\iota)} = \int_C d\eta \mathcal{G}_a(\eta) C_{\nu s}^{(\iota)}(\eta) \exp\{\mathcal{N}_s \mathcal{S}_{\iota s}(\eta)\}, \quad (53)$$

the integration path  $C$  on the complex plane  $\eta = \eta_r + i\eta_i$  is along the line, defined by  $\text{Im} [\alpha_0 + 2(g_{01}^{(s)} g_{10}^{(s)} / \beta)^{1/2} \eta] = 0$ , while

$$\mathcal{N}_s = \frac{\pi D}{|\Lambda_L|}, \quad \mathcal{S}_{\iota s}(\eta) = -i(|\Lambda_L|/\Lambda_L) \left[ p\eta + (-1)^{\iota+1} \sqrt{1 + \eta^2} \right]. \quad (54)$$

We assume that the crystal thickness  $D \gg |\Lambda_L|/\pi$  and the dispersion

$$\sigma \gg 2\sqrt{\frac{|\Lambda_L|}{\pi D}} |\Delta\vartheta|. \quad (55)$$

This allows us to estimate the integral (53) by the saddle-point method (for details see [9]). The saddle points determined by the equation  $\mathcal{S}'_{\iota}(\eta) = 0$  are

$$\eta_0^{(\iota)} = (-1)^\iota \eta_0, \quad \eta_0 = \frac{p}{\sqrt{1-p^2}}. \quad (56)$$

The amplitudes  $C_\nu^{(\iota)} = C_\nu^{(\iota)}(\eta_0^{(\iota)})$  in the saddle points take the form

$$C_0^{(\iota)} = \frac{1}{2} (1+p), \quad C_1^{(\iota)} = \frac{(-1)^\iota}{2} \left( \frac{g_{10}}{g_{01}} \beta \right)^{\frac{1}{2}} \sqrt{1-p^2}. \quad (57)$$

In general, the angular distribution (37) in the saddle points is represented by different factors

$$\mathcal{G}_1 \equiv \mathcal{G}_a(\eta_0^{(1)}) = \frac{1}{(2\pi\eta^2)^{1/4}} \exp\left\{-\frac{(\eta_0 + \Delta\eta)^2}{4\eta^2}\right\}, \quad \mathcal{G}_2 \equiv \mathcal{G}_a(\eta_0^{(2)}) = \frac{1}{(2\pi\eta^2)^{1/4}} \exp\left\{-\frac{(\eta_0 - \Delta\eta)^2}{4\eta^2}\right\}, \quad (58)$$

which only coincide in the case of exact Bragg resonance.

Employing standard formulas of the saddle-point method [14], one gets the wave function of photons in any point  $\mathbf{r} \approx \mathbf{r}_S$  close to the scanning slit. For the refracted  $\gamma$ -quanta with fixed frequency  $\omega$  the wave function is

$$\Psi_{\omega s}^{(0)}(\mathbf{r}) = \frac{1}{2} \frac{\mathbf{A}_{0s}(p)\Phi(p)}{(1-p^2)^{1/4}} \left(\frac{1+p}{1-p}\right)^{\frac{1}{2}} \sqrt{\frac{2\Lambda_L}{D}} \left[e^{i\zeta(p)} + e^{-i\zeta(p)}\right] e^{i\boldsymbol{\kappa}_0 \mathbf{r}} \quad (59)$$

and for the diffracted those

$$\Psi_{\omega s}^{(1)}(\mathbf{r}) = \frac{1}{2} \frac{\mathbf{A}_{1s}(p)\Phi(p)}{(1-p^2)^{1/4}} \sqrt{\frac{2\Lambda_L}{D}} \left[e^{i\zeta(p)} - e^{-i\zeta(p)}\right] e^{i\boldsymbol{\kappa}_1 \mathbf{r}},$$

where the function  $\zeta(p)$ , depending on the phases  $\phi_\nu = \arg \mathcal{G}_\nu$ , is given by

$$\zeta(p) = \frac{\pi D}{\Lambda_L} \sqrt{1-p^2} + \frac{\phi_2 - \phi_1}{2} + ib + \frac{\pi}{4} \quad (60)$$

with

$$b = \frac{1}{2} \ln \left| \frac{\mathcal{G}_1}{\mathcal{G}_2} \right|, \quad (61)$$

whereas the amplitudes  $\mathbf{A}_{\nu s}(p)$  are

$$\mathbf{A}_{0s}(p) = -\mathbf{e}_{0s} \sqrt{\hbar\omega} (\mathcal{G}_1 \mathcal{G}_2)^{1/2} \sqrt{\Delta\vartheta}, \quad \mathbf{A}_{1s}(p) = -\mathbf{e}_{1s} \sqrt{\hbar\omega} (\mathcal{G}_1 \mathcal{G}_2)^{1/2} \sqrt{\Delta\vartheta} \left(\frac{g_{10}}{g_{01}} \beta\right)^{\frac{1}{2}}. \quad (62)$$

Corresponding intensities of the monochromatic  $\gamma$ -radiation are determined by

$$I_{\nu s}(p, \omega) = |\Psi_{\omega s}^{(\nu)}(\mathbf{r})|^2. \quad (63)$$

After introduction of the Authier's [3] notation

$$\frac{1}{\Lambda_L} = \frac{1}{\tau_L} + i \frac{1}{\sigma_L}, \quad (64)$$

we are led to the following intensity distribution through the basis of the Borrmann triangle ( $|p| < 1$ ) for the refracted beam:

$$I_{0s}(p, \omega) = \frac{|\mathbf{A}_{0s}(p)|^2}{\sqrt{1-p^2}} \left(\frac{1+p}{1-p}\right) e^{-\mu D} \frac{2|\Lambda_L|}{D} \times \left[ \sinh^2 \left( \frac{\pi D}{\sigma_L} \sqrt{1-p^2} + b \right) + \cos^2 \left( \frac{\pi D}{\tau_L} \sqrt{1-p^2} + \frac{\phi_2 - \phi_1}{2} + \frac{\pi}{4} \right) \right], \quad (65)$$

and for the diffracted beam:

$$I_{1s}(p, \omega) = \frac{|\mathbf{A}_{1s}(p)|^2}{\sqrt{1-p^2}} e^{-\mu D} \frac{2|\Lambda_L|}{D} \times \left[ \sinh^2 \left( \frac{\pi D}{\sigma_L} \sqrt{1-p^2} + b \right) + \sin^2 \left( \frac{\pi D}{\tau_L} \sqrt{1-p^2} + \frac{\phi_2 - \phi_1}{2} + \frac{\pi}{4} \right) \right], \quad (66)$$

where

$$\mu = \frac{1}{2} \left[ \frac{\mu_0}{\gamma_0} + \frac{\mu_1}{\gamma_1} + p \left( \frac{\mu_0}{\gamma_0} - \frac{\mu_1}{\gamma_1} \right) \right] \quad (67)$$

with

$$\mu_\nu = \kappa \text{Im}g_{\nu\nu} = \sigma_a(\boldsymbol{\kappa}_\nu)/v_0, \quad (68)$$

and  $\sigma_a(\boldsymbol{\kappa}_\nu)$  meaning the absorption cross sections by an elementary cell of  $\gamma$ -quanta, which incident slightly off Bragg position with the wave vectors  $\approx \boldsymbol{\kappa}_\nu$ . In accordance with the optical theorem [12] the absorption cross section is determined by the imaginary part of the coherent elastic scattering amplitude to zeroth angle:

$$\sigma_a(\boldsymbol{\kappa}_\nu) = \frac{4\pi}{\kappa} \text{Im}F(\boldsymbol{\kappa}_\nu, \boldsymbol{\kappa}_\nu). \quad (69)$$

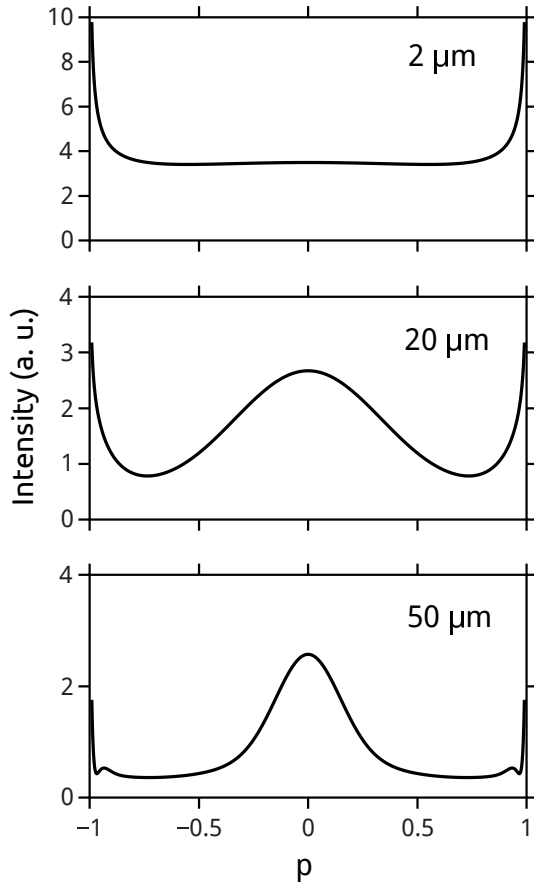


FIG. 2: Distribution of the Mössbauer beam intensity  $I_1(p)$ , diffracted in the tin film of different thickness, through the basis of the Borrmann triangle for the symmetric Laue diffraction at the Bragg angle  $\theta_B = 5^{\circ}6'$ , exact resonance  $\omega_0 = \omega'_0$ , and the 100% abundance by the Mössbauer isotope  $^{119}\text{Sn}$ .

In the opposite case of extremely narrow angular distribution, when

$$\sigma \ll 2\sqrt{\frac{|\Lambda_L|}{\pi D}}|\Delta\vartheta|, \quad (70)$$

the angular distribution (37) behaves like a delta function,

$$\mathcal{G}_a(\eta) \approx \delta(\eta - \bar{\eta}). \quad (71)$$

As a result, the integral in Eq. (52) is estimated as

$$\mathcal{I}_{\nu_s}^{(\iota)} = C_{\nu_s}^{(\iota)}(\bar{\eta}) \exp\{\mathcal{N}_s \mathcal{S}_{\iota_s}(\bar{\eta})\}. \quad (72)$$

At last, in the intermediate case of

$$\sigma \sim 2\sqrt{\frac{|\Lambda_L|}{\pi D}}|\Delta\vartheta|, \quad (73)$$

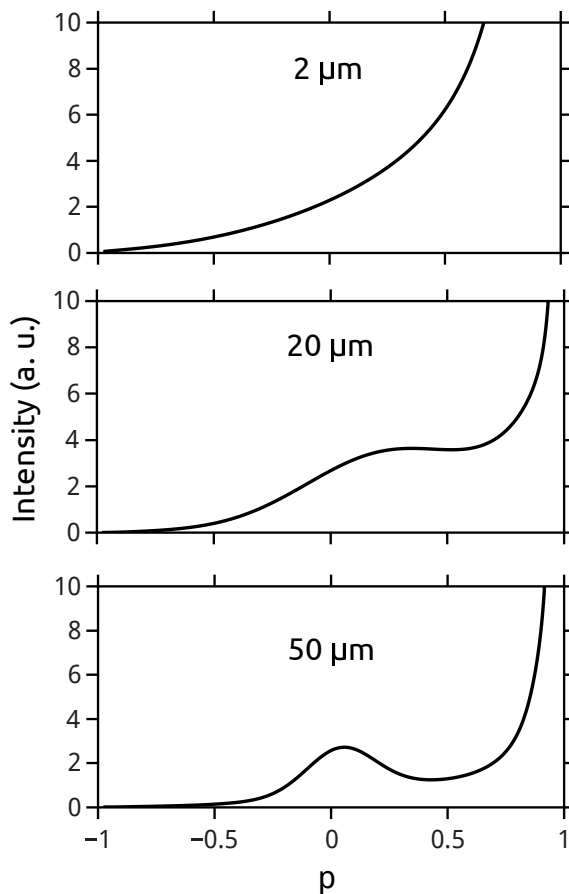


FIG. 3: The same as in Fig.2 but for the refracted beam  $I_0(p)$ .

the saddle points are determined by the equation

$$\frac{\eta - \bar{\eta}}{2\eta^2} + \mathcal{N}S'(\eta) = 0, \quad (74)$$

which reduces to an algebraic equation of the fourth order, giving already four saddle points.

It can be realized in experiments with synchrotron rays, when the angular dispersion achieves values  $\sigma \sim 0.1|\Delta\vartheta|$  [3].

Experimentally measured intensities of the  $\gamma$ -beams are obtained from (62), (63) by averaging them with the weight  $|G_e(\omega)|^2$ :

$$I_{\nu s}(p) = \int_0^\infty d\omega |G_e(\omega)|^2 I_{\nu s}(p; \omega). \quad (75)$$

#### IV. DISCUSSION

We developed general dynamical theory for the Laue diffraction of divergent beams of  $\gamma$ -quanta, taking into consideration both their scattering by atomic electrons and nuclei with low-lying excited levels. We confined ourselves by analysis of the two-wave case, allowing the analytical solution. The derived equations describe the refracted and diffracted beams for arbitrary orientation of the incident beam with respect to the Bragg resonance, i.e., for arbitrary deflection angle  $\theta'_B - \theta_0$ . Therefore they may be useful for interpretation of experiments taking the rocking curves, when the target rotates with respect to the incident beam. In the case when  $\theta'_B = \theta_0$  and respectively  $\phi_1 = \phi_2$  as well as  $b = 0$ , our equations (59)–(66) formally coincide with those given in the book [3]. However, our formulas depend on the scattering amplitudes on nuclei absent in the formalism of [3]. Moreover, they contain the realistic angular distribution of incident  $\gamma$ -photons. It is approximated by the Gaussian function with arbitrary width  $\sigma$ , which can

be of the same order or even less compared to the diffraction interval  $|\Delta\vartheta|$ . In principle, our final formulas remain the same if this Gaussian is replaced by any other function  $G_a(\theta)$  normalized by

$$\int_{-\infty}^{\infty} G_a^2(\theta) d\theta = 1. \quad (76)$$

Note also that according to derived formulae (65), (66) the deviation of the incident beam orientation  $\theta_0$  from the Bragg angle  $\theta_B$  leads to a shift of the Pendellösung fringe.

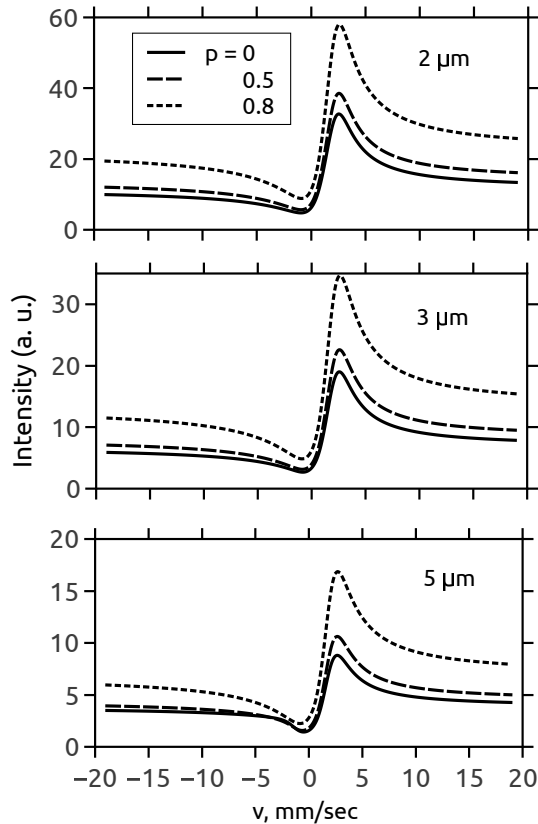


FIG. 4: The Mössbauer spectrum of the diffracted beam versus the relative motion velocity of the Mössbauer source and the target for different positions of the scanning slit  $p$ .

We illustrated our theory by analysis of the Mössbauer diffraction, assuming the nuclear sublevels to be unsplit, that simplifies consideration of the polarizations of  $\gamma$ -quanta. In particular, this is realized in the nuclei  $^{119}\text{Sn}$  with M1 transitions and transition energy  $E_0 = 23.8$  keV. The Mössbauer diffraction in tin single crystal has been observed by Voitovetskii et al. [15], studying the suppression of inelastic channels and reactions [4]. We performed numerical calculations for the symmetric Laue diffraction in the tin crystal film (see Figs. 2-5), choosing the same parameters as in the experiments reported in [15]. Namely, we consider the first-order reflection by the (020) planes with the Bragg angle  $\theta_B = 5^{\circ}6'$  and put the temperature  $T = 110$  K, when the ratio of the resonant nuclear amplitude  $|f_{res}^N|$  to the Rayleigh one  $f^R$  equals 3.2 and the ratio of the absorption coefficients  $\mu_N/\mu_e = 167$  [15]. Taking into account that the Debye temperature of tin  $\Theta_D = 200$  K we found the Lamb-Mössbauer factor to be  $e^{-W} = 0.48$  at  $T = 110$  K, which enabled us to get the nuclear scattering amplitude. All the curves are calculated in the Kato's approximation  $\sigma \gg |\Delta\vartheta|$ . All the curves drawn in Figs. 2-4 are calculated for the 100% abundance by  $^{119}\text{Sn}$ . The results presented in Figs. 2, 3 and 5 correspond to exact nuclear resonance, when  $\omega_0 = \omega'_0$ .

The calculated intensities of the diffracted beam  $I_1(p)$  are shown in Fig. 2 as a function of the parameter  $p$ , ranging from -1 to +1 for the film thicknesses  $D = 2, 20$  and  $50 \mu\text{m}$ . The corresponding curves for the refracted beam are given in Fig. 3. Here we observe the same behavior as in the case of x-ray diffraction. Namely, in thin weakly absorbing crystal there is a growth of the diffracted intensity to the edges of the Borrmann triangle  $p = \pm 1$ . With increasing film thickness, as the absorption grows, there appears a bump in the middle of the triangle ( $p = 0$ ). It can be explained that in strongly absorbing crystal the energy of  $\gamma$ -rays flows mainly along the reflecting planes (see also [2]).

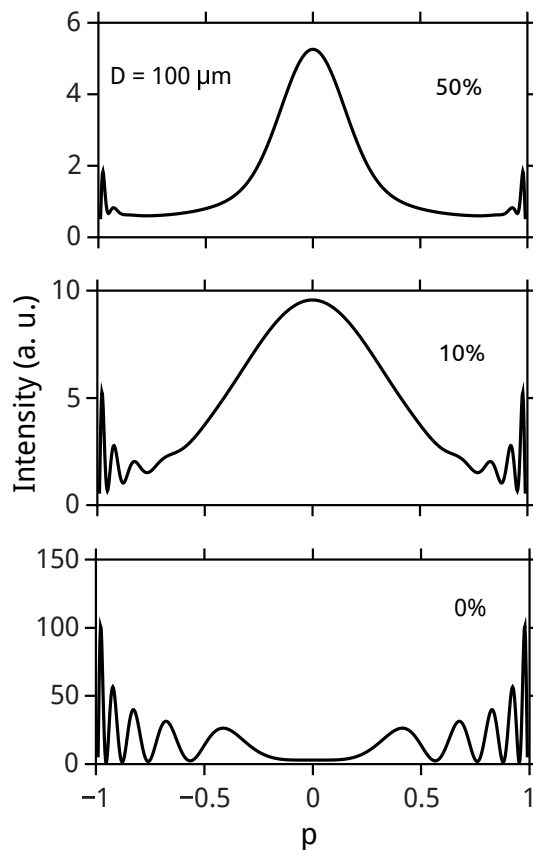


FIG. 5: Dependence of the intensity of diffracted radiation  $I_1(p)$  on  $p$  for concentrations of the Mössbauer isotope  $^{119}\text{Sn}$   $c_0 = 0.5$ ,  $0.1$  and  $0$ .

Dependence of the diffracted beam intensity on the relative velocity of the Mössbauer emitter and the target is analyzed in Fig. 4, where the crystal thickness is taken  $D = 2$ ,  $3$  and  $5 \mu\text{m}$ . The intensity curves manifest a characteristic asymmetry, caused by interference of the waves coherently scattered by the atomic electrons and the waves scattered by the nuclei. These results well agree with the observations of Voitovetskii et al. [15].

The diffracted wave intensity  $I_1(p)$  versus the concentration of the Mössbauer isotope  $c_0$  is displayed in Fig. 5 for the same tin crystal but with thickness  $D = 100 \mu\text{m}$  and concentrations  $c_0 = 0.5$ ,  $0.1$  and  $0$ . We see that with lowering  $c_0$  there appears fringe structure of the curve  $I_1(p)$ , which becomes most clear in the case  $c_0 = 0$ , corresponding to pure Rayleigh scattering of the Mössbauer radiation. With growing  $c_0$  the oscillations of  $I_1(p)$  are only conserved at the edges of the Borrmann triangle. For  $c_0 = 1$  oscillations of the curves  $I_1(p)$  are absent.

Thus, in the Rayleigh scattering of Mössbauer radiation experiments one can observe the intensity oscillations of the diffracted waves. Numerical calculations show the introduction of the angular distribution with  $\sigma \sim |\Delta\vartheta|$  leads to significant distortion of these curves. Specifically, the diffraction curve collapses to single peak at  $p = 0$  when the ratio  $\sigma/|\Delta\vartheta|$  tends to zero.

Our theory may be useful in the structure analysis of crystals and especially in studies of crystal defects analogous to [16]. Application of the Mössbauer spectroscopy in such studies has great advantage compared to standard x-ray optics due to extremely narrow frequency distribution of Mössbauer radiation.

- 
- [1] W.H.Zachariasen, *Theory of X-ray Diffraction in Crystals* (Wiley, New York, 1945).
  - [2] B.W.Batterman, H.Cole, Dynamical diffraction of X Rays by perfect crystals, *Rev. Mod. Phys.* **36**, 681 (1964).
  - [3] André Authier, *Dynamical Theory of X-ray Diffraction* (Oxford University Press Inc., New York, 2001).
  - [4] A.M.Afanas'ev, Yu.Kagan, Suppression of inelastic channels in resonant nuclear scattering in crystals, *Sov. Phys. JETP* **21**, 215 (1965).
  - [5] A.Ya.Dzyublik, Effect of forced vibrations on scattering of X-Rays and Mössbauer radiation by a crystal, *phys. stat. sol.*

- (b) **123**, 53 (1984); **134**, 503 (1986).
- [6] N.Kato, The energy flow of X-rays in an ideally perfect crystal: comparison between theory and experiments, *Acta Cryst.* **13**, 349 (1960).
- [7] A.Ya.Dzyublik, V.Yu.Spivak, Laue diffraction of spherical Mössbauer waves, *Ukr. J. Phys.* **61**, 826 (2016).
- [8] A.Ya.Dzyublik, V.I.Slisenko, V.V.Mykhaylovskyy, Symmetric Laue diffraction of spherical neutron waves in absorbing crystals, *Ukr. J. Phys.* **63**, 174 (2018).
- [9] A.Ya.Dzyublik, V.V.Mykhaylovskyy, V.Yu.Spivak, Peculiarities of Laue diffraction of neutrons in strongly absorbing crystals, *Zh. Eksp. Teor. Fiz.* **155**, 413 (2019); arXiv:1902.02051v1 [cond-mat.mtrl-sci]; *JETP* **128**, 355 (2019).
- [10] J.Bialynicki-Birula, On the wave function of the photon, *Acta Phys. Polonica* **86**, 97 (1994)
- [11] M.L.Goldberger, K.M.Watson, *Collision Theory*, (J. Wiley, New York, 1964).
- [12] A.G.Sitenko, *Scattering Theory* (Vishcha Shkola, Kiev, 1975; Shpringer, Berlin Heidelberg, 1999).
- [13] V.A.Belyakov, Diffraction of Mössbauer gamma rays in crystals, *Soviet Phys. Uspekhi* **18**, 267 (1975).
- [14] M.A.Lavrentiev, B.V.Shabat, *Methods of the Theory of Functions of Complex Variable* (Nauka, Moscow, 1973).
- [15] V.K.Voitovetskii et al., Diffraction of resonance  $\gamma$  rays by nuclei and electrons in tin crystals, *Soviet Phys. JETP* **27**, 729 (1968).
- [16] V.I.Khrupa, D.O.Grigoryev, A.Ya.Dzyublik, Structure perfection study of crystals containing micro- and macrodistortions by x-ray acoustic method, *Acta Phys. Polonica A* **86**, 597 (1994).